Influence of bioactive particles and onium salt on the physicochemical properties of experimental infiltrants

Caroline MATHIAS[a] (iD)
Rafael Soares GOMES[a] (iD)
Carmem Silvia PFEIFER[b] (iD)
Priscila Regis PEDREIRA[a] (iD)
Janaina Emanuela DAMASCENO[a] (iD)
Giselle Maria MARCHI[a] (iD)

[a] Universidade Estadual de Campinas – Unicamp, Piracicaba Dental School, Department of Restorative Dentistry, Piracicaba, SP, Brazil.

[b] Oregon Health and Science University, Division of Biomaterials and Biomechanics, Department of Restorative Dentistry, Portland, OR, USA.

Corresponding Author:
Caroline Mathias
E-mail: caroline.mathias@hotmail.com

Abstract: This study evaluated physicochemical properties of experimental infiltrants after addition of hydroxyapatite nanoparticles (HAp) or 58S bioactive glass (BAG) and diphenyliodonium hexafluorophosphate (DPI). The resin matrix was composed of TEGDMA/Bis-EMA (3:1), 0.5 mol% CQ, and 1 mol% EDAB. The blends received or not 0.5 mol% DPI and 10% wt BAG or HAp. Icon was used as commercial control. The groups were characterized by XRD, FT-IR spectrometry, and SEM before and after simulated body fluid (SBF) immersion for up to 7 days. Polymerization kinetics (n =3), water sorption and solubility (n=10), and viscosity (n = 3) were surveyed. For polymerization kinetics, the samples were polymerized for 5 min and the data were obtained from 40 s and 5 min. Statistical analysis was made using ANOVA and Tukey's test (a = 0.05). After 7 days of SBF immersion, XRD and FT-IR showed that the HAp crystalline phase was present only in the HAp groups. A lower degree of conversion (DC) and polymerization rate were observed for the Icon and BAG groups, whereas HAp showed higher values. For the BAG group, DPI increased polymerization rate and DC in 40 s. After 5 min, all groups presented DC above 80%. In groups with particles, the HAp groups exhibited higher viscosity, whereas DPI groups showed a decrease in viscosity. Icon had the highest water sorption. To conclude, BAG neither improved the physicochemical properties studied, nor did it show bioactive properties. The addition of DPI reduced viscosity caused by particle addition and also attenuated the DC decrease caused by BAG addition. The addition of bioactive particles to infiltrants should be seen with caution because they increase viscosity and may not bring major clinical improvements that justify their use. DPI might be indicated only if any component is added to the infiltrant to act as a compensation mechanism.

Keywords: Hydroxyapatites; Resins, Synthetic; Dental Materials.

Introduction

It has been reported that infiltrant resins can successfully be used to treat early carious lesions, such as white spots.[1-3] This approach is used to create a mechanical barrier into the body of the lesion to halt the progression of demineralization by acidogenic bacteria.[3] The

main component of the infiltrant is TEGDMA, a monomer with low mechanical properties and high susceptibility to hydrolytic degradation[4-6] and, therefore, modifications have been suggested to improve the properties of these materials. [7-9] For example, the addition of BisEMA has been suggested to increase the hydrophobic character and to improve mechanical properties.[4] In addition, the incorporation of onium salts such as diphenyliodonium hexafluorophosphate (DPI) into methacrylates has been reported to improve mechanical properties[10-12] via an increase in reactivity and degree of conversion of the system.[13,14] Thus, it is suggested that DPI can combine with camphorquinone (CQ), allowing initiating and increasing the polymerization reaction of the material.[10-14]

Other reinforcement strategies include the addition of antimicrobial and remineralizing compounds with the potential for reduced risk of recurrent caries.[15,16] Some of those are also bioactive particles, which play a role in decreasing the likelihood for recurrence of caries in the infiltrated region, may also improve the physicochemical properties of materials by acting as fillers.[17,18] Therefore, some compositions of bioactive glasses and nanohydroxyapatite particles have been tested in infiltrants and resin composites.[17-19]

Bioactive glasses are highly biocompatible silicate-based materials that can stimulate a biological response in the human body without producing inflammation and toxicity, and they are widely used in dentistry.[20-23] The hydroxyapatite layer is formed when the bioactive glass is exposed to an aqueous environment, such as the oral environment. Therefore, there is an ion exchange with the oral medium that allows for remineralization when the bioactive glass is incorporated into restorative materials and that is also related to antimicrobial activity [23,24]. 58S bioactive glass (60 mol% SiO_2, 36 mol% CaO, and 4 mol% P_2O_5) is the best-known bioactive glass produced by the sol-gel method. In the sol-gel method, higher purity can be achieved because there is greater control during the manufacture of the bioactive glass, in which the temperature is lowered to decrease the possibility of contamination.[25]

By contrast, the production of bioactive glasses by the conventional method, which employs high temperatures (1,250–1,400°C) has numerous disadvantages, including the difficulty in avoiding impurities.[21] This melting method was used in the development of the first bioactive glass, 45S5 (46.1 mol% SiO^2, 24.4 mol% Na_2O, 26.9 mol% CaO, and 2.6 mol% P_2O_5), known as Bioglassâ and widely studied[26]. However, studies have demonstrated that high purity of the particle is required for an optimal bioactivity and the particles produced by the sol-gel method actually present increased bioactivity compared to those produced by melting[27] and, therefore, the 58S bioactive glass produced by the sol-gel method was chosen for this study.

Another particle that can be possibly incorporated into composites is hydroxyapatite [Hap, $Ca_{10}(PO_4)_6(OH)_2$] because of its biocompatibility, osteoconductivity, and bioactivity, which have been shown to be dependent on particle size.[19] It has been suggested that the inclusion of such particles in infiltrants would not impair the penetration of the material into the lesion pores and, furthermore, it could increase the degree of conversion and resistance against acid challenges.[19] It is important to highlight that bioactive materials applied to dental tissues have benefits related to mineral deposition on surfaces. In addition, they form a protective layer over dental tissues with chemical characteristics that resemble those of natural tissues, presenting biomimetic properties.[19,20,23,26]

Dental materials are exposed to many challenges in the oral cavity, such as the demineralization-remineralization cycle as the caries disease progresses. Therefore, it is desirable that resin infiltrants have antimicrobial and remineralizing properties through the release of previously selected ions. Few studies have shown that the incorporation of bioactive particles improves the mechanical properties of experimental infiltrants,[17,19] so there is a lack of information in the literature about the chemical, physical, and bioactivity performance of infiltrants containing 58S bioactive glass or HAp nanoparticle. In addition, there is no information about whether the potential increase in conversion

achieved with the incorporation of DPI would be able to improve the resistance to hydrolytic degradation of infiltrants containing bioactive particles. Therefore, the objective of this study was to evaluate the influence of DPI and the addition of 58S bioactive glass and hydroxyapatite nanoparticles on the physical properties and bioactivity of experimental infiltrants. The hypotheses of the study were: a) the 58S bioactive glass particle would be able to exhibit bioactivity after SBF immersion; b) the addition of bioactive particles would increase the degree of conversion of infiltrants; c) DPI would be able to decrease water sorption and solubility and viscosity of infiltrants.

Methodology

Synthesis of 58S bioactive glass by the sol-gel method

58S bioactive glass (BAG) was composed of 60 mol% SiO_2, 36 mol% CaO, and 4 mol% P_2O_5. A solution containing 98% tetraethoxysilane (TEOS, Si $(OC_2H_5)_4$ (Sigma-Aldrich, Steinheim, Germany), deionized water (H_2O), 99.8% triethylphosphate (TEP, $(C_2H_5)_3PO_4$) (Sigma-Aldrich, Steinheim, Germany), and calcium nitrate tetrahydrate ($CaN_2O_6 * 4H_2O$) was kept under continuous stirring at 600 rpm until gelation. To do that, 13.2 mL of TEOS, used as precursor for silica (SiO), was added to 1.6 mL of nitric acid and 9.5 mL of water, and stirred for 30 min. Thereafter, 0.7 mL of TEP, used as precursor for phosphate, was added to the mixture dispensed with a micropipette set to that volume in one go, and 5.8 g of calcium nitrate tetrahydrate was added after 20 min of stirring. After that, 0.7 mL of TEP, used as phosphate precursor, was added to the mixture, and 5.8 g of calcium nitrate tetrahydrate was added after 20 min of stirring. To achieve the complete dissolution of calcium nitrate and hydrolysis reaction, the stirring was maintained until gelation. The solution was oven-dried at 180 °C for 6 h followed by the stabilization cycle in a furnace at 700 °C for 18 h. The dried products were pulverized in an agate mortar with a pestle and passed through a granulometric sieve (Tyler 325 mesh - ASTM 325),

which corresponds to an aperture of 45 micrometers (ISO 3310/1) so that only particles smaller than that size could be selected.[21,33]

Experimental infiltrant formulation

Experimental infiltrants were made in a dark room with yellow light and controlled temperature (25ºC), based on previous studies.[10] The resin blends were made with a magnetic stirrer mixing 75 wt% triethylene-glycol-dimethacrylate (TEGDMA), 25 wt% ethoxy bisphenol A glycidyl dimethacrylate (BisEMA), 0.5 wt% camphoroquinone (CQ), and 1 wt% ethyl 4-dimethylaminebenzoate (EDAB) for 24 h to ensure homogeneity. This blend was divided into six experimental groups according to the photoinitiator system and unsilanized bioactive particles used, as shown in Table 1. The Icon infiltrant (DMG, Hamburg, Germany) was used as commercial control.

After addition of 10 wt% hydroxyapatite (Sigma-Aldrich, Steinheim, Germany, < 200 nm) or 10 wt% 58S bioactive glass (£ 45 mm), experimental infiltrants were mixed with a magnetic stirrer for 24 h at an average speed of 100 rpm. After that, the mixtures were placed in a tub attached to a vacuum pump (Quimis Aparelhos Científicos Ltda., Diadema, Brazil) for 20 min to eliminate air bubbles. Subsequently, they were placed in an ultrasonic bath for 30 min to avoid agglutination of the particles. All experimental infiltrants were stored under refrigeration at 4°C.

SBF immersion

To evaluate the ability of forming hydroxyapatite, disc-shaped resin specimens were made (9.5 mm x 2 mm) from a silicone matrix. The infiltrant was deposited into the matrix, covered with a polyester strip, and polymerized with a LED light source (Valo cordless, Ultradent, South Jordan, USA) for 40 s. Initially, XRD, FT-IR, and SEM (JSM-5600LV, Jeol, Boston, USA) were performed for the qualitative analysis. After that, the specimens were immersed in SBF solution (in 10^{-3} mol: 142 Na^+, 5 K^+, 1.5 Mg^{2+}, 2.5 Ca^{2+}, 147.8 Cl^-, 4.2 HCO_3^-, 1.0 HPO_4^{2-}, and 0.5 SO_4^{2-}, pH=7.4) for 6 h, for 1, 3, and

Table 1. Composition of groups according to photoinitiator system and bioactive particles used.

Groups	Composition
B-Neat	(3:1) TEGDMA/BisEMA, 0.5 mol% CQ/ 1 mol% EDAB
T-Neat	(3:1) TEGDMA/BisEMA, 0.5 mol% CQ/ 1 mol% EDAB/ 0.5 mol% DPI
B-HAp	(3:1) TEGDMA/BisEMA, 0.5 mol% CQ/ 1 mol% EDAB + 10 wt% Hydroxyapatite
T-HAp	(3:1) TEGDMA/BisEMA, 0.5 mol% CQ/ 1 mol% EDAB/ 0.5 mol% DPI + 10 wt% Hydroxyapatite
B-BAG	(3:1) TEGDMA/BisEMA, 0.5 mol% CQ/ 1 mol% EDAB + 10 wt% 58S Bioactive glass
T-BAG	(3:1) TEGDMA/BisEMA, 0.5 mol% CQ/ 1 mol% EDAB/ 0.5 mol% DPI + 10 wt% 58S Bioactive glass
Icon	TEGDMA resin-based

All materials were from Sigma-Aldrich (Steinheim, Germany). TEGDMA: triethylene glycol dimethacrylate; Bis-EMA: ethoxy bisphenol A glycidyl dimethacrylate; CQ: camphorquinone; EDAB: ethyl 4- (dimethylamino) benzoate; DPI: diphenyliodonium hexafluorophosphate; B: binary; T: ternary.

7 days using 7 mL of SBF for the specimen at 37°C. The SBF solution was replaced every 3 days to avoid increasing the concentration of cations in the solution. Thereafter, the specimens were rinsed under running distilled water for about 10 s to remove SBF and any precipitation that had occurred. After being rinsed, they were placed in an oven at 37°C until the XRD analysis was performed. The FT-IR and SEM analyses were performed using the specimens not subjected to SBF and specimens subjected to SBF for 7 days.

The XRD analysis was performed using an X-ray diffractometer, Bruker D8 Advance 3kW (Karlsruhe, Germany) equipped with Cu Ka tube, 40 kV voltage, and 30 mA. This analysis was performed at room temperature and the area analyzed was 0.7 cm², and the .raw files were converted to .xy by using the PowDLL software version 2.991 and, after that, the graphs were plotted using the ORIGIN 8 PRO software. For the FT-IR spectroscopy analysis, the specimens were ground on an agate mortar and pressed on discs with KBr at a ratio between 1:30 (spciemen:KBr). The spectra were recorded in the 4000–400 cm⁻¹ range with 32 scans at 4 cm⁻¹ resolution using the FT- IR (Nicolet 6700 FTIR, Thermo Scientific, Pittsburgh, USA).

Photopolymerization reaction kinetics and degree of conversion

Degree of conversion and polymerization kinetics were monitored by near-infrared using a spectrometer (Nicolet 6700 FTIR, Thermo Scientific, Pittsburgh, USA). Infiltrant specimens were placed in silicone rubber molds ($n = 3$; $\varnothing = 5.0$ mm; $h = 0.5$ mm) sandwiched between glass slides. FT-IR spectra (2 scans per spectrum, 4 cm⁻¹ resolution, with collection speed of two spectra/s) were collected during 330 s. The peak area corresponding to the vinyl stretching overtone (6165 cm⁻¹) was used. The materials were photoactivated with 390 mW/cm² because of the distance of 3 cm from the LED device to the specimen surface, for 5 min (Valo cordless, Ultradent, South Jordan, UT, USA). Degree of conversion (DC) was calculated from the ratio of peak area according the formula:

$$DC = \left(1 - \frac{monomer\ area}{polymer\ area} \right) \times 100$$

The rate of polymerization (Rp) was calculated as the first derivative of the conversion vs. the time curve. Kinetic parameters such as maximum rate of polymerization Rp_{max} (%/s) and DC at Rp_{max} (%) were determined.

Water sorption and solubility

The water sorption and solubility tests were based on ISO 4049:2009, except for specimen dimensions. Eight resin infiltrant disks were made for each group using a polyvinyl siloxane mold (Express XT Putty Soft-VPS; 3M ESPE, St. Paul, USA) of 5 mm in diameter and 1 mm thick, and The water sorption and solubility tests were based

on ISO 4049:2009, except for specimen dimensions. Eight resin infiltrant disks were made for each group using a polyvinyl siloxane mold (Express XT Putty Soft-VPS; 3M ESPE, St. Paul, USA) of 5 mm in diameter and 1 mm thick, and The water sorption and solubility tests were based on ISO 4049:2009, except for specimen dimensions. Eight resin infiltrant disks were made for each group using a polyvinyl siloxane mold (Express XT Putty Soft-VPS; 3M ESPE, St. Paul, USA) of 5 mm in diameter and 1 mm thick, and The water sorption and solubility tests were based on ISO 4049:2009, except for specimen dimensions. Eight resin infiltrant disks were made for each group using a polyvinyl siloxane mold (Express XT Putty Soft-VPS; 3M ESPE, St. Paul, USA) of 5 mm in diameter and 1 mm thick, and The water sorption and solubility tests were based on ISO 4049:2009, except for specimen dimensions. Eight resin infiltrant disks were made for each group using a polyvinyl siloxane mold (Express XT Putty Soft-VPS; 3M ESPE, St. Paul, USA) of 5 mm in diameter and 1 mm thick, and the water sorption (WS) and solubility (Sol) tests were performed based on ISO 4049:2009, except for specimen dimensions and, consequently, deionized water volume. Resin infiltrant discs were made (n = 10) using a polyvinyl siloxane mold (Express XT Putty Soft-VPS; 3M ESPE, St. Paul, USA), (5 mm x 1 mm), covered with a polyester strip and photoactivated for 40 s (Valo corded; Ultradent, South Jordan, UT, USA). The specimens were dried in a desiccator containing silica gel (37°C) for 7 days and weighed daily on a precision analytical balance (AUW220D Shimadzu, Kyoto, Japan) until a constant mass ($m1$) was obtained (i.e., when the weight varied less than 0.1 mg within 24 h). The volume (v) of all discs was calculated using a digital caliper (Mitutoyo, Kanagawa, Japan) and the specimens were immersed in 1.5 mL of deionized water at 37°C using microtubes (Flex-tube; Eppendorf, Hamburg, Germany). After 7 days, the specimens were rinsed under running distilled water, blot-dried, weighed ($m2$), and subsequently returned to the desiccator (silica gel, 37°C). These samples were weighed daily until

a new constant mass was achieved ($m3$). Water sorption and solubility were calculated using the following formulas respectively:

$$Ws = \frac{(m2 - m3)}{v} \quad \text{and} \quad Sol = \frac{(m1 - m3)}{v}.$$

Viscosity assessment before light-curing

All groups were subjected to rheological analysis using a cone-plate rheometer (ARES, TA Instruments, New Castle, USA). Approximately 1 g of each material was placed between 20-mm diameter plates, tested at 1Hz with a gap of 0.3 mm and shear rate ranging from 0.1 to 100 s^{-1} (n = 3). During the experiment, the graph of viscosity x velocity rate was built using TRIOS software (TA Instruments, New Castle, USA) coupled to the rheometer. To calculate viscosity, the mean of the three most linear points of the blue line on the graph for each specimen was considered.

Statistical analysis

The normality and homogeneity of the studied parameters were checked using the Shapiro-Wilk and Levene's tests, respectively. All groups presented normal distribution and homogeneity of variance. Statistical comparisons between the groups were made using analysis of variance (one-way ANOVA) and post-hoc comparisons by Tukey's test with a significance level of a = 0.05 using SPSS 23 (IBM Corp., Somers, USA).

The viscosities of the unfilled resins (n = 3) were determined in a viscometer (CAP 200+ Viscometer; Brookfield Engineering Laboratories, Middleboro, USA), at 2,684 g and 25°C.

Samples were held in place for 5 s before being submitted to shear for 30 s. Shear rates of 667 s)1 (small-diameter spindle) or 2,667 s)1 (high-diameter spindle) were used for higher-viscosity and lower-viscosity samples, respectively. The viscosities of the unfilled resins (n = 3) were determined in a viscometer (CAP 200+ Viscometer; Brookfield Engineering Laboratories, USA), at 2,684 g and 25°C. Samples were held in place for 5 s before being

submitted to shear for 30 s. Shear rates of 667 s)1 (small-diameter spindle) or 2,667 s)1 (high-diameter spindle) were used for higher-viscosity and lower-viscosity samples, respectively.

Results

SBF immersion

The XRD spectrum for the infiltrants at baseline is shown in Figure 1. The XRD spectra of the groups without particles, as expected, shows no crystalline peaks. Instead, their spectra are characteristic of polymers, with broad bands distributed in a wide range (2θ), instead of a high-intensity narrower peak. The BAG groups presented similar spectra compared to no-particle groups, given that 58s particles are also of a disorderly and amorphous nature when not subjected to a crystallization process. In contrast, the HAp groups showed several typical sharp peaks, which combined with the similar ratio between 2θ position of 32.166 (112 plane) and 32.92 (300 plane). No difference was observed in the XRD spectra
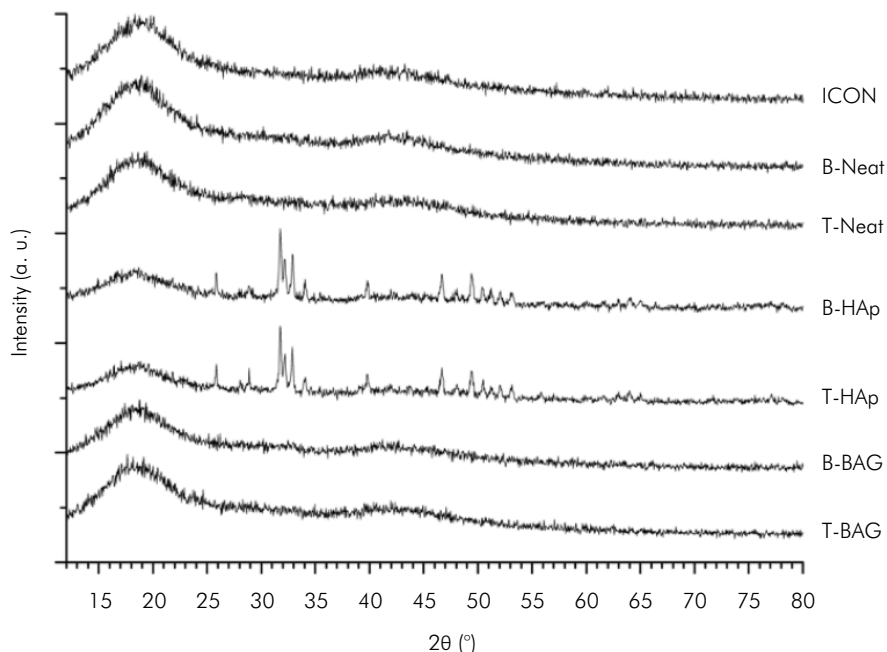
after 7 days of SBF immersion (Figure 2), nor in any of the evaluated days (6 h, 1 day and 3 days), for all groups.

The infrared transmittance spectra of the specimens before and after 7 days in SBF immersion are shown in Figure 3. The BAG groups did not show crystallinity after SBF immersion due to the absence of the PO_4^{3-} functional group, following the same results of the XRD analysis. A peak at 3448 cm^{-1} in the broad band in the 3100–3600 cm^{-1} spectral region is presented assigned to the hydroxyl group stretching mode [34]. The other main peak is presented at 1,730 cm^{-1} assigned to C = O stretch. The groups with particles showed a slight difference in the peaks. HAp groups showed peaks in the 1040 cm^{-1} and 560 cm^{-1} regions assigned to the asymmetric stretching mode of the PO_4^{3-} functional group [35], while BAG groups showed a peak at 1080–1090 cm^{-1}, which corresponds to Si-O-Si stretching.

The representative SEM images (Figure 4) show the surface of Icon and infiltrant discs before
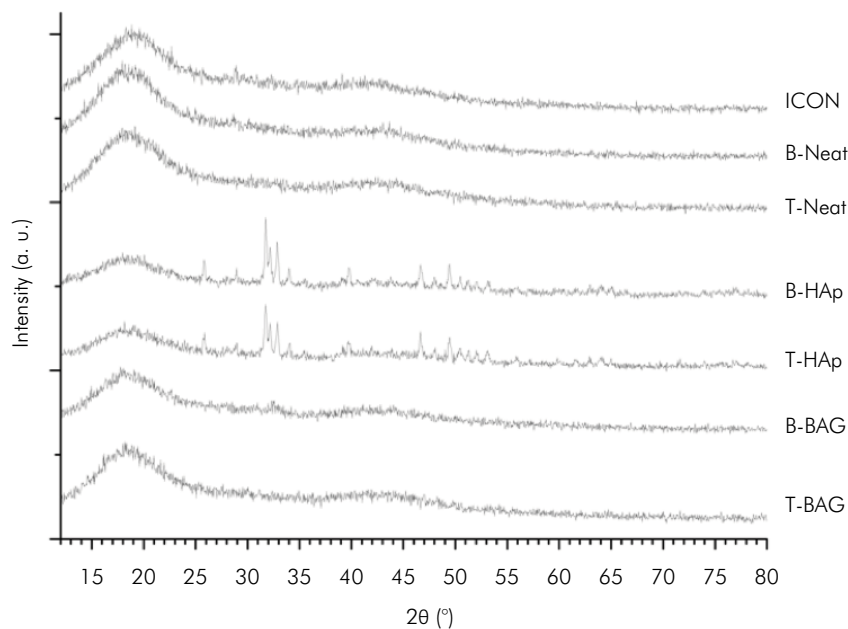
Figure 1. XRD patterns obtained from all groups at baseline (no SBF immersion). A broad band around 15~20(2θ), indicating an amorphous pattern in the ICON, Neat, and BAG groups. Additionally, HAp groups show sharp peaks around ~32(2θ) and minor peaks between ~45 and 50(2θ), indicating that its structure exhibited crystalline characteristics, as expected, even prior to SBF immersion.

Figure 2. XRD patterns obtained from all groups after 7 days of SBF immersion. No difference was observed compared to before immersion. The same amorphous characteristic appears in the ICON, Neat, and BAG groups, indicating their non-bioactive behavior in SBF solution. HAp groups show no difference in the previously presented hydroxyapatite peaks, indicating no reaction between those groups and the SBF solution.

(left-side images) and after 7 days of SBF immersion (right-side images). The images 4*e* and 4*f* show the presence of HAp nanoparticles. Also, the 58S BAG particles can be seen in the 4*g* and 4*h* images before and after 7 days of SBF immersion.

Photopolymerization reaction kinetics and degree of conversion

At 40 s of photoactivation, Icon and B-BAG groups had the lowest conversion values, which were below 50% (p < 0.05) (DC at 40 s, Table 2). At the same time, the Neat and HAp groups did not differ significantly in the degree of conversion, ranging from 70.9 (1.28) to 77.6 (3.12) (p > 0.05). After 5 min of photoactivation, all groups presented conversion values higher than 80% (Figure 5). The maximum rate of polymerization (Rpmax, Table 2) exhibited the same trend as DC at 40 s, with Icon and B-BAG group presenting slower rates (p < 0.05) (Figure 6).

Water sorption and solubility

Icon presented the highest value of water sorption among the tested groups (p<0.05). The lowest values of water sorption were found in the groups composed of the binary photoinitiator system (p < 0.05) (Table 3). No statistically significant difference was found for the solubility values (p > 0.05) (Table 3).

Viscosity assessment before light-curing

The viscosities of the unfilled resins (n = 3) were determined in a viscometer (CAP 200+ Viscometer; Brookfield Engineering Laboratories, USA), at 2,684 g and 25°C. Samples were held in place for 5 s before being submitted to shear for 30 s. Shear rates of 667 s)1 (small-diameter spindle) or 2,667 s)1 (high-diameter spindle) were used for higher-viscosity and lower-viscosity samples, respectively.

All experimental infiltrants presented statistically significant increase in viscosity compared to Icon
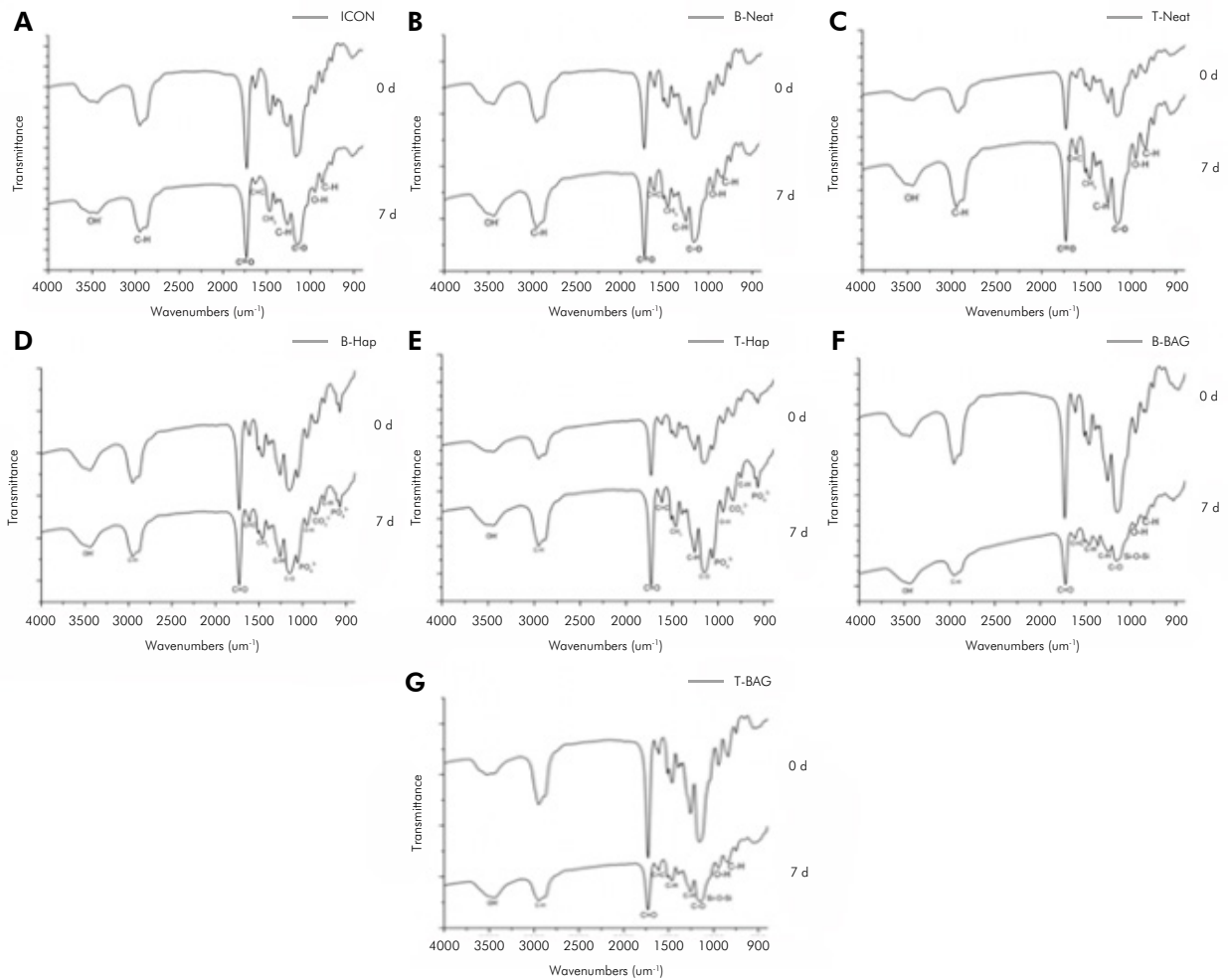
Figure 3. FT-IR patterns obtained from all groups at baseline and after 7 days of SFB immersion. a) FT-IR patterns for the Icon group; b) FT-IR patterns for the B-Neat group; c) FT-IR patterns for the T-Neat group; d) FT-IR patterns for the B-HAp group; e) FT-IR patterns for the T-HAp group; f) FT-IR patterns for the B-BAG group; g) FT-IR patterns for the T-BAG group. BAG groups showed a common peak at 1,080–1,090 cm-1 assigned to the Si-O-Si stretching mode, while HAp showed peaks in the region of 1040 cm-1 and 560 cm-1 assigned to the asymmetric stretching mode of PO_4^{3-}. As in XRD, no difference was observed in the FT-IR peak patterns before and after SBF immersion.

($p < 0.05$) (Figure 7). The B-HAp group presented the highest value among the groups ($p < 0.05$) and no statistical difference was found between the groups without filler ($p > 0.05$).

Discussion

The experimental infiltrants in this study presented some changes in the physical properties tested after incorporation of bioactive particles and DPI. The first hypothesis of this study could not be accepted because it was not possible to confirm the

bioactivity of 58S bioactivity glass. The incorporation of bioactive particles into infiltrants is innovative and there are only a few studies that have investigated the addition of particles to infiltrants.[6,17,19] One of those studies has tested the incorporation of 10% of bioactive particles: HAp, amorphous calcium phosphate (ACP), zinc-modified bioactive glass (BAG-Zn), bioglass 45S5 (BAG), and β-tricalcium phosphate modified calcium silicate cements (β-TCP) in experimental infiltrant (similar composition to the one used in this study), but only mechanical properties were evaluated.[17] They found that the
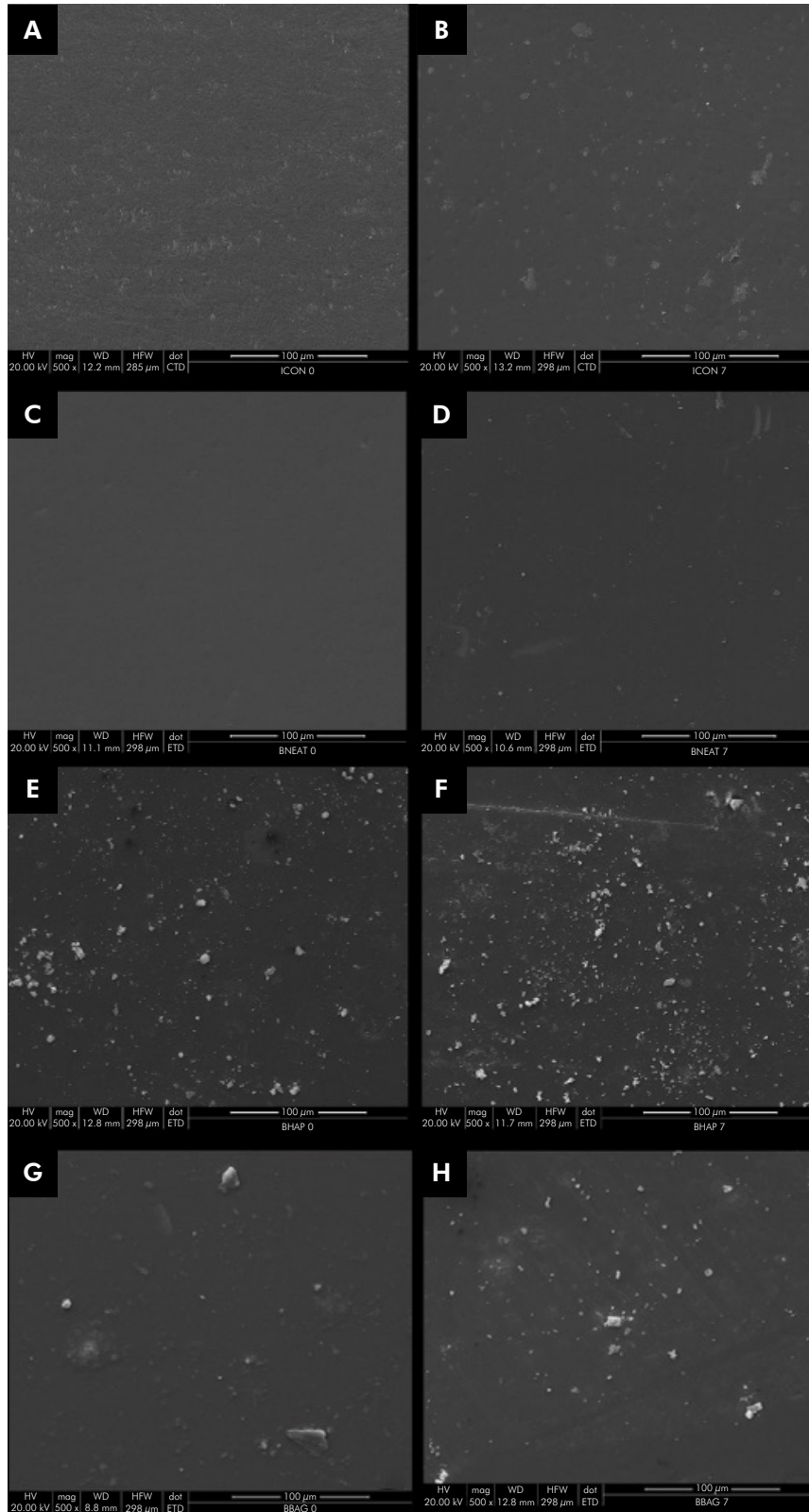
Figure 4. SEM representative images of the ICON, Neat, BAG, and HAp groups at baseline (a,c,e and g, respectively) and after 7 days of SBF immersion (b,d,f and h, respectively). Image shows absence of particles in the ICON and Neat groups before and after SBF immersion, indicating its non-bioactivity. BAG and HAp groups show particles prior to SBF immersion that were not modified after immersion, indicating also an absence of bioactive behavior.

incorporation of bioactive particles into experimental resin infiltrants did not have statistical difference in DC in comparison to the experimental infiltrant without particles. Therefore, addition of all bioactive particles, except for ACP, reduced water sorption and solubility because, after adding filler to the resin material, the organic matrix content was reduced, thus decreasing hydrolytic degradation.[17] Additionally, the crystalline phase of HAp nanorods investigated by Andrade et al.[12] was characterized by XDR and FT-IR only before its incorporation into the material. To our knowledge, no information was found in the literature regarding the functionality of the bioactive particles after incorporation into the infiltrants.

The antimicrobial effect of bioactive glass materials is promoted by the dissolution of ions released by the bioactive glass, favoring an increase of the pH of the interfacial solution and making it infeasible for several bacterial species.[33] Considering
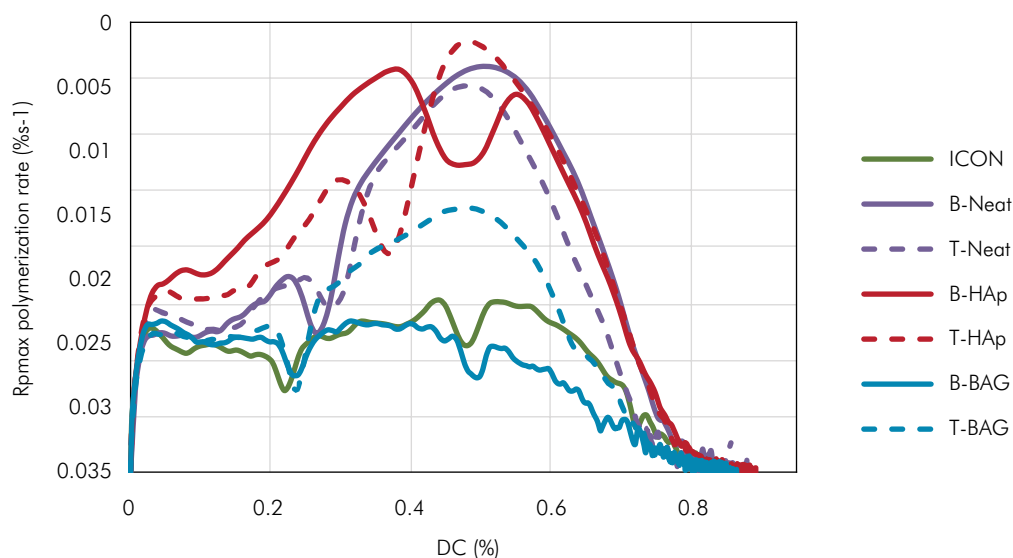
Table 2. Mean and standard deviation of maximum rate of polymerization (Rpmax), degree of conversion at maximum rate of polymerization (DC at Rpmax), DC at 40s and Final DC according to the groups.

Groups	Rpmax (% s-1)	DC at Rpmax (%)	DC at 40s (%)	Final DC (%)
	Mean (SD)	Mean (SD)	Mean (SD)	Mean (SD)
Icon	1.59E-02 (8.41E-04)[c]	46.26 (2.02)[b]	44.94 (1.85)[c]	84.32 (1.15)[a]
B-Neat	3.66E-02 (2.41E-03)[a]	50.31 (1.74)[ab]	74.01 (3.28)[a]	84.05 (0.84)[ab]
T-Neat	3.45E-02 (1.61E-03)[a]	47.98 (1.30)[b]	70.86 (1.28)[a]	84.63 (0.62)[a]
B-HAp	3.42E-02 (3.44E-03)[a]	54.97 (4.38)[a]	77.60 (3.12)[a]	83.70 (0.88)[ab]
T-HAp	4.01E-02 (2.92E-03)[a]	46.97 (2.41)[b]	75.58 (3.87)[a]	84.65 (1.13)[a]
B-BAG	1.36E-02 (1.66E-03)[c]	33.73 (1.59)[c]	47.12 (2.95)[c]	81.42 (1.01)[b]
T-BAG	2.35E-02 (9.35E-04)[b]	48.21 (2.23)[a]	57.95 (2.36)[b]	83.93 (1.02)[ab]

Values followed by the same letter in the same column are statistically similar (One-way ANOVA/Tukeys test, p < 0.05).
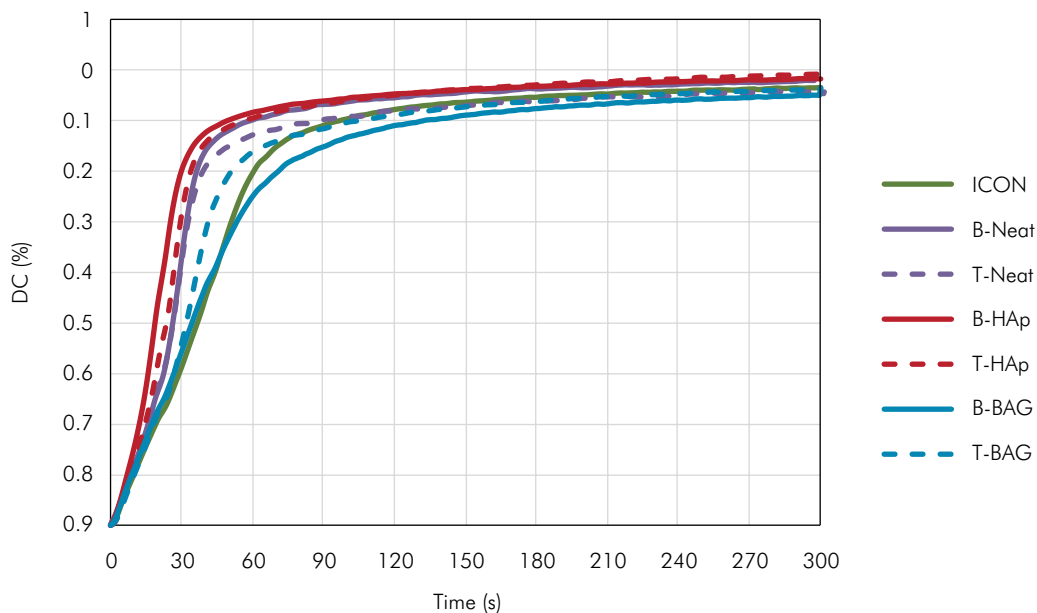
Figure 5. Degree of conversion (DC) x time of all groups. ICON and BAG groups exhibit a delay in the DC over time with significant lower DC at 40 s (p < 0.05). This difference was getting shorter overtime until all groups surpass 80% of DC after a high photopolymerization exposure.

Figure 6. Rate of polymerization (Rpmax) x degree of conversion (DC) of all groups. The maximum rate of polymerization of all groups appear in the range of 33–55% of DC. Neat and HAp groups exhibit a parabolic-like behavior, while ICON and B-BAG groups maintain a more linear curve until Rpmax.

**Table 3.** Mean and standard deviation of water sorption and solubility according to the groups ($\mu g/mm^3$).

Groups	Water Sorption (SD)	Solubility (SD)
Icon	49.58 (5.84)[a]	5.16 (3.03)[a]
B-Neat	30.55 (3.63)[c]	6.13 (2.01)[a]
T-Neat	38.63 (3.88)[b]	5.35 (1.96)[a]
B-HAp	35.18 (3.76)[bc]	7.55 (1.64)[a]
T-HAp	38.48 (4.36)[b]	8.14 (3.10)[a]
B-BAG	36.29 (4.37)[bc]	7.22 (1.96)[a]
T-BAG	38.78 (4.13)[b]	6.39 (2.33)[a]

Values followed by the same letter in the same column are statistically similar (One-way ANOVA/Tukeys test, $p < 0.05$).

studies that investigated the antimicrobial effect of bioactive glasses in dimethacylate-based dental resin, perhaps the addition of only 10% of BAG to the infiltrants may not be enough to have had its bioactivity demonstrated by XDR and FT-IR in this study.[18,21,36] According to a study that tested the incorporation of 10 or 20 wt% of BAG into experimental adhesives, bioactivity was only observed at 20 wt% of nanoparticles,[36] which agrees with the findings of the present study. Once the addition of particles to infiltrants increases their

viscosity, the authors recommend the incorporation of at most 15 wt% particles to allow for adequate penetrability of the infiltrant.[37] Additionally, it is important to mention that several studies which tested bioactive particles did it in the human body, either by graft or scaffolds, a situation that is different from incorporating it into a monomeric matrix.[21] Even though the particles were not silanized, their possible retention within the resin matrix could be also a reason for the lack of bioactivity. Contributing to this assumption, SEM images showed few BAG particles on the surface with no noticeably relevant difference after SBF immersion for all groups.

Monomer size, mobility, and functionality are factors that can influence the rate of polymerization of the material.[38] The rate of polymerization of all groups presented a double kinetic profile formed by two phases. This may indicate that, at least for some of the binary/ternary compositions (either with two monomers or with the addition of particles), polymerization-induced heterogeneous phase formation occurred, with each of the different phases polymerizing at different rates.[39] In addition, TEGDMA has a strong tendency to form primary cyclizations, in which the pendant double bond reacts intramolecularly.[39-41] This, in turn, may lead to the
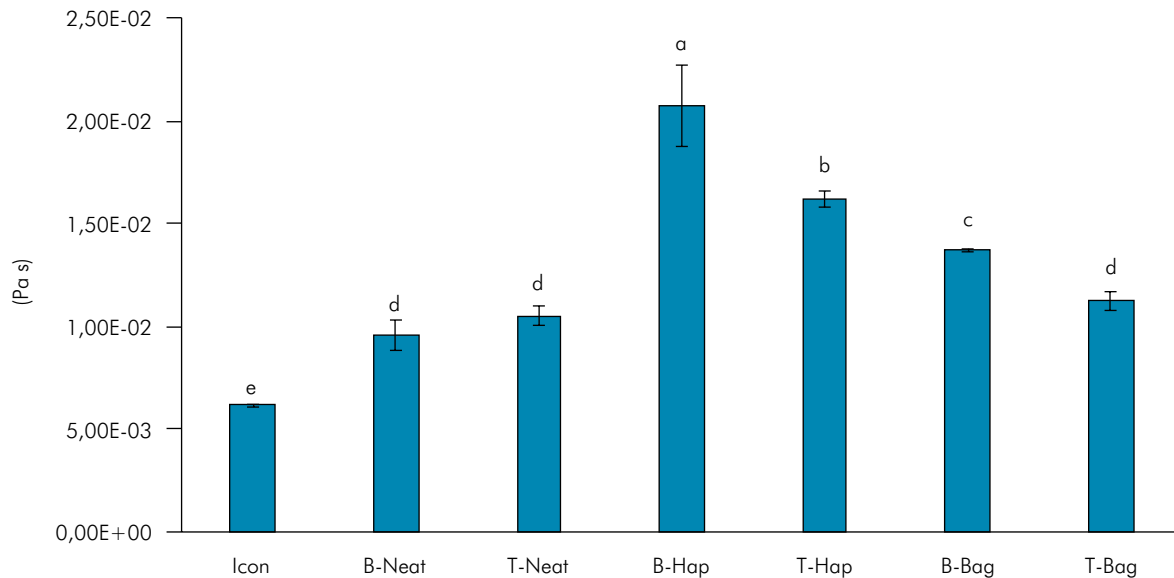
Figure 7. Mean and standard deviation for viscosity according to the groups. Particle-containing groups tend to show higher viscosity than the others. Values followed by the same letter are statistically similar (One-way ANOVA/Tukey's test, $p < 0.05$).

formation of heterogeneity even in single monomer formulations. As all groups were composed of at least 75% of TEGDMA, it is likely that both of those factors played a role in leading to the double kinetic profile observed.

Icon presented the lowest DC after 40 s of photoactivation, which is the time of curing recommended by the manufacturer. Studies have found about 50–56% of degree of conversion, considering 60 s of photoactivation for Icon. [17,42] The values of conversion found in this study ($44.94 \pm 1.85\%$) were lower than the ones previously reported. The low DC of Icon in both studies could be explained by the high amount of TEGDMA (> 90%) in the material and also because of the concentration and type of initiators, which are unknown. Besides, comparing this study with others, the difference could be explained by the photoactivation time (40 s), differently from the other studies (60 s).[17,42] Therefore, the addition of other low-viscosity, but more rigid monomers such as Bis-EMA, could improve the polymerization of dimethacrylates, resulting in stiffer crosslinks which, in turn, leads to better mechanical properties.[17,38]

The presence of HAp increased the DC at 40 s compared to BAG particles, which presented lower DC than the Neat groups. Therefore, the second hypothesis of this study was rejected. This finding could be explained by the use of highly crystalline nanoparticles, such as HAp, its diffraction and less scattering effects may increase the rate of polymerization.[19] However, the addition of BAG reduced the Rpmax to 1.36E-02 (1.66E-03) %.s[-1], compared to 3.66E-02 (2.41E-03) %.s[-1] for the experimental control. The DC at Rpmax was lower, indicating that the vitrification happened earlier in conversion, resulting in lower overall DC. This reduction can be explained by the inhibition of free-radical polymerization by electron transfer to oxides on the surface of particles.[43].This may occur when the particles are unsilanized, so the oxide radicals formed are not able to continue the reaction at the near-room temperature.[43] Regarding DC at 40 s, all groups were similar, except for Icon and when BAG was present. It seems that the addition of DPI was not much helpful if the rate was lower, because as DPI is a third component of the photoinitiator system, the reaction became more sensitive and the activation energy increased. Furthermore, it is known that DPI has greater potential to compensate for negative effects on the polymerization of resin materials that contain hydrophilic monomers and/

or solvents (such as HEMA and ethanol), as seen in the results of the studies by Mathias[10] and Sauro[44] than in monomeric bases containing crosslinking monomers as in the present study.

The lowest viscosity was found for Icon because of the low molecular weight of TEGDMA and other differences in the composition that are unknown, as they are not informed by the manufacturer. Some rheological studies showed that viscosity increases exponentially when smaller particles are added to the matrix.[45] Therefore, the presence of HAp and BAG increased the viscosity as expected, and B-HAp presented the highest viscosity because of its smaller size (< 200 nm). However, DPI was able to compensate for this increase, reducing the viscosity and rendering T-BAG group similar to the Neat groups.[10] Possibly, DPI had some interaction with the particles used in this study, maybe influencing the particle distribution and agglomeration, making the material more fluid. Another study[10] found that the presence of DPI decreased the contact angle, a property that may be related to the viscosity of materials of a similar monomeric base and containing ethanol as solvent. Owing to the lack of studies that explore the rheological properties of resin materials containing DPI, further investigations are suggested, as DPI seems to compensate for the increase in the viscosity of the material in the presence of particles, which could improve wettability and/or increase the surface free energy during the infiltration process into the dental enamel. Although higher viscosity was found for the HAp groups, this did not influence DC, nor B-BAG, which presented the lowest DC and did not have higher viscosity than did the HAp groups. However, it is possible to obtain similar DC from blends with different viscosities, once the blends have different structures and reactivities. Moreover, the intermolecular and intramolecular interactions in the uncured material and during the photopolymerization are not the same.[46] In this study, it seems that the interaction between the particles and the light had more influence on the DC than did the viscosity of the material. In addition, further studies should be performed to verify whether this increase in viscosity interferes with the penetration of such infiltrants into demineralized enamel.

Considering that the partition coefficient in water (log P) of TEGDMA is 1.42 and BisEMA is 6.01, with lower log P values associated with more hydrophilic materials, it is not surprising that Icon presented higher water sorption because of the higher concentration of TEDGMA in its composition. Water sorption is also related to the conversion achieved by the polymer, besides the nature of its network,[41] and the lower conversion achieved by that material; therefore, this also helps explain the WS/Sol results. However, the B-BAG group also presented lowest DC at 40 s (photoactivation time for WS/Sol tests), but it was not the one with the greatest WS. Therefore, the log P seemed to have been more influential in water uptake. It is important to note that a low DC does not mean high concentration of unreacted monomer, as it could mean a lot of pendant bonds or presence of oligomers that were not extracted in water.[43]

When DPI is present, WS was slightly greater for Neat groups. However, no difference was found for solubility, regardless of the presence of the bioactive particles or DPI. These findings corroborate those of another study in which the same matrix composition and the addition of 0.5 mol% of DPI were tested, leading to increased WS but not to an increase in the solubility of the materials.[10] According to studies, the amount and hydrophilicity of the leachates present in the material also have influence on solubility values, rather than only the amount of water uptake by the network. Therefore, pendant double bonds that favor WS might not contribute to the leachability of monomers and oligomers, which are tied to the network.[41] Thus, the third hypothesis of this study was rejected, once DPI did not decrease WS and solubility and only decreased the viscosity when bioactive particles were present.

The production of bioactive materials with remineralizing or antibacterial effects needs to be investigated to expand the indications of infiltrants, as for pit and fissures, and provide better restorative materials in general. In the present study, it was not possible to verify the penetration depth of the materials tested in a carious lesion, and it was not

possible to use other methodologies that would help verify bioactivity. Thus, further studies should demonstrate the bioactivity of other types of particles to find the better balance between these effects in the oral cavity, physicomechanical properties, and also the penetrability of the infiltrants. Moreover, other methodologies such as Raman spectroscopy could be helpful to assess the bioactivity of the material. Also, atomic absorption spectroscopy could measure the release of calcium, which could indicate a bioactive behavior.

Conclusions

According to the present study, BAG neither improved the physicochemical properties studied, nor did it show bioactive properties. The addition of DPI reduced viscosity caused by particle addition and attenuated the decrease in DC caused by BAG addition. SW/Sol were not affected by the presence of particles; however, given the methodologies used, it was not possible to verify the bioactivity of the materials tested.

References

1. Jia L, Stawarczyk B, Schmidlin PR, Attin T, Wiegand A. Effect of caries infiltrant application on shear bond strength of different adhesive systems to sound and demineralized enamel. J Adhes Dent. 2012 Dec;14(6):569-74.

2. Belli R, Rahiotis C, Schubert EW, Baratieri LN, Petschelt A, Lohbauer U. Wear and morphology of infiltrated white spot lesions. J Dent. 2011 May;39(5):376-85. https://doi.org/10.1016/j.jdent.2011.02.009

3. Meyer-Lueckel H, Bitter K, Paris S. Randomized controlled clinical trial on proximal caries infiltration: three-year follow-up. Caries Res. 2012;46(6):544-8. https://doi.org/10.1159/000341807

4. Araújo GS, Sfalcin RA, Araújo TG, Alonso RC, Puppin-Rontani RM. Evaluation of polymerization characteristics and penetration into enamel caries lesions of experimental infiltrants. J Dent. 2013 Nov;41(11):1014-9. https://doi.org/10.1016/j.jdent.2013.08.019

5. Paris S, Lausch J, Selje T, Dörfer CE, Meyer-Lueckel H. Comparison of sealant and infiltrant penetration into pit and fissure caries lesions in vitro. J Dent. 2014 Apr;42(4):432-8. https://doi.org/10.1016/j.jdent.2014.01.006

6. Lausch J, Askar H, Paris S, Meyer-Lueckel H. Micro-filled resin infiltration of fissure caries lesions in vitro. J Dent. 2017 Feb;57:73-6. https://doi.org/10.1016/j.jdent.2016.12.010

7. Paris S, Meyer-Lueckel H. Inhibition of caries progression by resin infiltration in situ. Caries Res. 2010;44(1):47-54. https://doi.org/10.1159/000275917

8. Brambilla E, Ionescu A, Mazzoni A, Cadenaro M, Gagliani M, Ferraroni M, et al. Hydrophilicity of dentin bonding systems influences in vitro Streptococcus mutans biofilm formation. Dent Mater. 2014 Aug;30(8):926-35. https://doi.org/10.1016/j.dental.2014.05.009

9. Khalichi P, Cvitkovitch DG, Santerre JP. Effect of composite resin biodegradation products on oral streptococcal growth. Biomaterials. 2004 Nov;25(24):5467-72. https://doi.org/10.1016/j.biomaterials.2003.12.056

10. Mathias C, Gomes RS, Dressano D, Braga RR, Aguiar FH, Marchi GM. Effect of diphenyliodonium hexafluorophosphate salt on experimental infiltrants containing different diluents. Odontology. 2019 Apr;107(2):202-8. https://doi.org/10.1007/s10266-018-0391-0

11. Dressano D, Palialol AR, Xavier TA, Braga RR, Oxman JD, Watts DC, et al. Effect of diphenyliodonium hexafluorophosphate on the physical and chemical properties of ethanolic solvated resins containing camphorquinone and 1-phenyl-1,2-propanedione sensitizers as initiators. Dent Mater. 2016 Jun;32(6):756-64. https://doi.org/10.1016/j.dental.2016.03.010

12. Andrade KM, Palialol AR, Lancellotti AC, Aguiar FH, Watts DC, Gonçalves LS, et al. Effect of diphenyliodonium hexafluorphosphate on resin cements containing different concentrations of ethyl 4-(dimethylamino)benzoate and 2-(dimethylamino)ethyl methacrylate as co-initiators. Dent Mater. 2016 Jun;32(6):749-55. https://doi.org/10.1016/j.dental.2016.03.014

13. Ogliari FA, Ely C, Petzhold CL, Demarco FF, Piva E. Onium salt improves the polymerization kinetics in an experimental dental adhesive resin. J Dent. 2007 Jul;35(7):583-7. https://doi.org/10.1016/j.jdent.2007.04.001

14. Sauro S, Sadhvik V, Sanjukta D. Development and assessment of experimental dental polymers with enhanced polymerization crosslink density and resistance to fluid permeability based on ethoxylated-Bisphenol-A-dimethacrylates and 2-Hydroxyethyl methacrylate. Eur Polym J. 2012;48(8):1466-74. https://doi.org/10.1016/j.eurpolymj.2012.05.013

15. Chiari MD, Rodrigues MC, Xavier TA, Souza EM, Arana-Chavez VE, Braga RR. Mechanical properties and ion release from bioactive restorative composites containing glass fillers and calcium phosphate nano-structured particles. Dent Mater. 2015 Jun;31(6):726-33. https://doi.org/10.1016/j.dental.2015.03.015

16. Degrazia FW, Leitune VC, Takimi AS, Collares FM, Sauro S. Physicochemical and bioactive properties of innovative resin-based materials containing functional halloysite-nanotubes fillers. Dent Mater. 2016 Sep;32(9):1133-43. https://doi.org/10.1016/j.dental.2016.06.012

17. Sfalcin RA, Correr AB, Morbidelli LR, Araújo TG, Feitosa VP, Correr-Sobrinho L, et al. Influence of bioactive particles on the chemical-mechanical properties of experimental enamel resin infiltrants. Clin Oral Investig. 2017 Jul;21(6):2143-51. https://doi.org/10.1007/s00784-016-2005-y

18. Khvostenko D, Hilton TJ, Ferracane JL, Mitchell JC, Kruzic JJ. Bioactive glass fillers reduce bacterial penetration into marginal gaps for composite restorations. Dent Mater. 2016 Jan;32(1):73-81. https://doi.org/10.1016/j.dental.2015.10.007

19. Andrade Neto DM, Carvalho EV, Rodrigues EA, Feitosa VP, Sauro S, Mele G, et al. Novel hydroxyapatite nanorods improve anti-caries efficacy of enamel infiltrants. Dent Mater. 2016 Jun;32(6):784-93. https://doi.org/10.1016/j.dental.2016.03.026

20. Boccaccini AR, Erol M, Stark WJ, Mohn D, Hong Z, Mano JF. Polymer/bioactive glass nanocomposites for biomedical applications: A review. Compos Sci Technol. 2010;70(13):1764-76. https://doi.org/10.1016/j.compscitech.2010.06.002

21. Abbasi Z, Me B, Mh S, Bagheri R. Bioactive Glasses in Dentistry : A Review, J. Glas. Dent Rev. 2015;2:1-9.

22. Peltola T, Jokinen M, Rahiala H, Levänen E, Rosenholm JB, Kangasniemi I, et al. Calcium phosphate formation on porous sol-gel-derived SiO_2 and $CaO-P_2O_5-SiO_2$ substrates in vitro. J Biomed Mater Res. 1999 Jan;44(1):12-21. https://doi.org/10.1002/(SICI)1097-4636(199901)44:1<12::AID-JBM2>3.0.CO;2-E

23. Pereira MM, Hench LL. Mechanisms of hydroxyapatite formation on porous gel-silica substrates. J Sol-Gel Sci Technol. 1996;7(1-2):59-68. https://doi.org/10.1007/BF00401884

24. Hyun HK, Salehi S, Ferracane JL. Biofilm formation affects surface properties of novel bioactive glass-containing composites. Dent Mater. 2015 Dec;31(12):1599-608. https://doi.org/10.1016/j.dental.2015.10.011

25. Goudouri OM, Kontonasaki E, Theocharidou A, Papadopoulou L, Chatzistavrou X, Koidis P, et al. In Vitro Bioactivity Studies of Sol-Gel Derived Dental Ceramics/Bioactive Glass Composites in Periodically Renewed Biomimetic Solution. Volume 1. Bioceramics Development and Applications; 2011. p. 4.

26. Hench LL. The story of Bioglass. J Mater Sci Mater Med. 2006 Nov;17(11):967-78. https://doi.org/10.1007/s10856-006-0432-z

27. Li R, Clark AE, Hench LL. An investigation of bioactive glass powders by sol-gel processing. J Appl Biomater. 1991;2(4):231-9. https://doi.org/10.1002/jab.770020403

28. Sepulveda P, Jones JR, Hench LL. Characterization of melt-derived 45S5 and sol-gel-derived 58S bioactive glasses. J Biomed Mater Res. 2001;58(6):734-40. https://doi.org/10.1002/jbm.10026

29. Pereira MM, Clark AE, Hench LL. Calcium phosphate formation on sol-gel-derived bioactive glasses in vitro. J Biomed Mater Res. 1994 Jun;28(6):693-8. https://doi.org/10.1002/jbm.820280606

30. Goel A, Kapoor S, Rajagopal RR, Pascual MJ, Kim HW, Ferreira JM. Alkali-free bioactive glasses for bone tissue engineering: a preliminary investigation. Acta Biomater. 2012 Jan;8(1):361-72. https://doi.org/10.1016/j.actbio.2011.08.026

31. Kapoor S, Semitela Â, Goel A, Xiang Y, Du J, Lourenço AH, et al. Understanding the composition-structure-bioactivity relationships in diopside ($CaO·MgO·2SiO_2$)-tricalcium phosphate ($3CaO·P_2O_5$) glass system. Acta Biomater. 2015 Mar;15:210-26. https://doi.org/10.1016/j.actbio.2015.01.001

32. Schmitz SI, Widholz B, Essers C, Becker M, Tulyaganov DU, Moghaddam A, et al. Superior biocompatibility and comparable osteoinductive properties: sodium-reduced fluoride-containing bioactive glass belonging to the CaO-MgO-SiO2 system as a promising alternative to 45S5 bioactive glass. Bioact Mater. 2020 Jan;5(1):55-65. https://doi.org/10.1016/j.bioactmat.2019.12.005

33. Abbasi Z, Bahrololoum ME, Bagheri R, Shariat MH. Characterization of the bioactive and mechanical behavior of dental ceramic/sol-gel derived bioactive glass mixtures. J Mech Behav Biomed Mater. 2016 Feb;54(54):115-22. https://doi.org/10.1016/j.jmbbm.2015.09.025

34. Berzina-Cimdina L, Borodajenko N. Research of calcium phosphates using fourier transform infrared spectroscopy. In: Theophanides , ed. Infrared spectroscopy. IntechOpen; 2012. p. 123-48.

35. Chandrasekar, Arunseshan, S. Suresh Sagadevan, A. Dakshnamoorthy, Synthesis and characterization of nano-hydroxyapatite (n-HAP) using the wet chemical technique. Int J Phys Sci,2013 Aug;8(32):1639-45. https://doi.org/10.5897/IJPS2013.3990

36. Tauböck TT, Zehnder M,Schweizer T, Stark WJ, Attin T, Mohn D. Functionalizing a dentin bonding resin to become bioactive, Dent. Mater. 2014 Aug;30(8):868-75. https://doi.org/10.1016/j.dental.2014.05.029

37. Van Landuyt KL, Snauwaert J, De Munck J, Peumans M, Yoshida Y, Poitevin A, et al. Systematic review of the chemical composition of contemporary dental adhesives. Biomaterials. 2007 Sep;28(26):3757-85. https://doi.org/10.1016/j.biomaterials.2007.04.044

38. Asmussen E, Peutzfeldt A. Influence of composition on rate of polymerization contraction of light-curing resin composites. Acta Odontol Scand. 2002 Jun;60(3):146-50. https://doi.org/10.1080/000163502753740151

39. Pfeifer CS, Shelton ZR, Braga RR, Windmoller D, Machado JC, Stansbury JW. Characterization of dimethacrylate polymeric networks: a study of the crosslinked structure formed by monomers used in dental composites. Eur Polym J. 2011 Feb;47(2):162-70. https://doi.org/10.1016/j.eurpolymj.2010.11.007

40. Elliott JE, Bowman CN. Kinetics of primary cyclization reactions in cross-linked polymers: an analytical and numerical approach to heterogeneity in network formation. Macromolecules. 1999;32(25):8621-8. https://doi.org/10.1021/ma990797i.

41. Gajewski VE, Pfeifer CS, Fróes-Salgado NR, Boaro LC, Braga RR. Monomers used in resin composites: degree of conversion, mechanical properties and water sorption/solubility. Braz Dent J. 2012;23(5):508-14. https://doi.org/10.1590/S0103-64402012000500007

42. Inagaki LT, Alonso RC, Araújo GA, de Souza-Junior EJ, Anibal PC, Höfling JF, et al. Effect of monomer blend and chlorhexidine-adding on physical, mechanical and biological properties of experimental infiltrants. Dent Mater. 2016 Dec;32(12):e307-13. https://doi.org/10.1016/j.dental.2016.09.028

43. Par M, Tarle Z, Hickel R, Ilie N. Polymerization kinetics of experimental bioactive composites containing bioactive glass. J Dent. 2018 Sep;76:83-8. https://doi.org/10.1016/j.jdent.2018.06.012

44. Sauro S, Vijay S, Deb S. Development and assessment of experimental dental polymers with enhanced polymerisation, crosslink density and resistance to fluid permeability based on ethoxylated-Bisphenol-A-dimethacrylates and 2-Hydroxyethyl methacrylate. Eur Polym J. 2012;48(8):1466-74. https://doi.org/10.1016/j.eurpolymj.2012.05.013.

45. Lee JH, Um CM, Lee IB. Rheological properties of resin composites according to variations in monomer and filler composition. Dent Mater. 2006 Jun;22(6):515-26. https://doi.org/10.1016/j.dental.2005.05.008

46. Gonçalves F, Kawano Y, Pfeifer C, Stansbury JW, Braga RR. Influence of BisGMA, TEGDMA, and BisEMA contents on viscosity, conversion, and flexural strength of experimental resins and composites. Eur J Oral Sci. 2009 Aug;117(4):442-6. https://doi.org/10.1111/j.1600-0722.2009.00636.x